Published in IET Generation, Transmission & Distribution with doi: 10.1049/gtd2.12742

A Novel Newton-like Method with High Convergence Rate for Efficient Power-Flow Solution in Isolated Microgrids

Marcos Tostado-Véliz[1], Mohammad Bayat[2,3,*], Ali Asghar Ghadimi[2,3] and Francisco Jurado[1]

1. *Department of Electrical Engineering, University of Jaén, 23700 EPS Linares, Jaén, Spain (e-mail: mtostado@ujaen.es (M.T.-V), fjurado@ujaen.es (F.J.))*
2. *Department of Electrical Engineering, Faculty of Engineering, Arak University, Arak 38156-8-8349, Iran (e-mail: m-baiat@araku.ac.ir (M.B.) and a-ghadimi@araku.ac.ir (A.A.G.))*
3. *Research Institute of Renewable Energy, Arak University, Arak 38156-8-8349, Iran*

Correspondence: m-baiat@araku.ac.ir, +98 9102003116

Abstract- Power-Flow solution in isolated Microgrids has attracted notable attention recently, because these systems present various particularities compared with the traditional Power-Flow solution in large meshed transmission networks. In this sense, this paper develops a novel Newton-like Power-Flow solver for isolated Microgrids. The new proposal is based on the Modified Midpoint method and shows high convergence order with relatively low computational burden. These characteristics bring superior theoretical performance compared with the standard Newton-Raphson method and other high order techniques, which has been conventionally used. Extensive simulations are performed on various small-, and large-scale benchmark Microgrids under different loading conditions and R/X ratios. Results provided serve to confirm the theoretical features of the developed solver, outperforming the Newton-Raphson technique as well as other recently developed solvers in all the studied systems with acceptable reliability even under high stressed conditions.

Keywords: Power-Flow analysis, Newton-like methods, Computational efficiency, High convergence rate, Modified Midpoint method, Isolated microgrid

1 - Introduction

The Power-Flow (PF) is likely the most important computational tool in power system analysis [1]. Its applicability to conventional power systems have been well-studied, tackling ill-conditioned problems [2], very large-scale networks [3], distribution grids [4], computational efficiency [5], etc. In contrast, the PF problem for islanded microgrids (PF-IMGs) could be considered a few-explored issue. It is expected a growing emergence of this kind of systems, because its importance to further integrate renewable sources, electric vehicles and storage technologies [6]. In this regard, further research efforts should be conducted on investigating the PF-IMGs, in order to develop mature techniques and solvers able to manage with this problem efficiently.

The PF-IMGs present several particularities compared to the traditional PF problem, which make the conventional PF tools unsuitable for PF-IMGs. The most notorious difference between the two problems is the consideration of the system frequency as a non-constant parameter in IMGs. Accordingly, the use of the slack bus concept is no longer valid in IMGs. The most common approach to manage with this issue consists on considering the system frequency as a free variable. Thus, one obtains a system of nonlinear equations for which the state vector has a larger dimension, which can be solved by applying conventional approaches like Newton-like methods [7]-[9], the backward-forward sweep algorithm [10], trust region techniques [11] or metaheuristic methods [12]. Other authors have explored original algorithms to circumvent the frequency-variable behaviour of IMGs. Thus, the references [13], [14] proposed the loop-based iterative algorithms which aims at mimicking the conventional PF solution procedure. Thereby, a slack bus is randomly selected among all system buses. Then, the problem is iteratively solved until the power injections of the selected slack bus are zero.

The non-constant frequency feature of IMGs brings other related issues that must be addressed. For instance, since the system frequency is variable, the bus admittance matrix is not constant during the iterative PF solution, because the dependency of the impedance value with the frequency. In this sense, Kumar et al. [15] proposed a two-loop iterative algorithm which is capable to manage with a variable admittance matrix. Another category of references has treated with the control principle of distributed energy resources (DERs). Thus, while most of the authors considered the conventional droop-based control, other works have contemplated the isochronous operating mode [16], [17]. In the droop problem, the set of equation varies when a DER reaches its delivered power limits, which makes the solution of the system more complex. The authors in [18] posed an alternative formulation based on the Fischer-Burmeister method to manage with this issue.

In conventional systems, system operators require rapid PF tools, in order to obtain a solution as quickly as possible. This requirement results essential for multiple online applications such as security analysis [19]. The same exigency is expected to be demanded by microgrid operators, since multiple tools must be still online performed [20]. In this sense, as in conventional networks, the nonlinear PF technique required to solve the resulting system of equations supposes the main computational bottleneck. In this regard, the existing literature has been largely focused on applying the traditional Newton-Raphson (NR) technique. This solver has multiple advantages; however, a

plethora of algorithms have demonstrated computational superiority due to their high order of convergence. Such techniques are conventionally grouped in the family of high-order Newton-like (HONL) methods [5]. Unlike the NR, the HONL solvers present an order of convergence higher than two, so that they are expected to converge employing a fewer number of iterations. If together to this feature, the computational complexity of the method is light yet, the resulting algorithm should be more competitive than the conventional NR. Despite this salient feature and the variety of existing HONL techniques (e.g. see the literature review of [21]), the applicability of these methods to PF-IMGs has not been investigated yet. This work aims at filling this gap by developing a novel HONL solver for PF-IMGs based on the Modified Mid-Point (MMP) rule, which has been called High Order MMP (HOMMP) method. The novel technique presents a multi-step structure by which its order of convergence is equal to N+1 (where N is the number of steps), however, its computational effort is comparable to the conventional NR. Multiple simulations are performed on various benchmark test cases under different conditions, in order to compare the performance of the new proposal with other available PF solvers.

In the rest of this paper, Section 2 outlines the PF-IMGs and its solution using the NR. Section 3 describes the solution of the PF-IMGs with the developed HOMMP and proofs its convergence. Various numerical results are provided and analysed in Section 4. The article is concluded with Section 5.

2 - NR-based solution of the PF-IMGs

Throughout this paper, the formulation of the PF-IMGs used in [8], [9], and [20] with some modifications has been considered. This section is devoted on briefly explaining this formulation, without including unnecessary details, for which the reader is referred to the original references. Unlike the conventional PF, for which the constant-power load model is usually assumed, in IMGs it is necessary to consider the voltage-, and frequency-dependent characteristics of the loads, as follows

$$P_{Li(f,V_i)} = P_{Loi} \cdot \left(1 + k_{pfi}(f - f_o)\right) \cdot \left(\frac{V_i}{V_{oi}}\right)^{k_{pvi}} \tag{1}$$

$$Q_{Li(f,V_i)} = Q_{Loi} \cdot \left(1 + k_{qfi}(f - f_o)\right) \cdot \left(\frac{V_i}{V_{oi}}\right)^{k_{qvi}} \tag{2}$$

where the subscript i stands for the i^{th} system bus; P_{Li} and Q_{Li} are the active and reactive actual loads, respectively; P_{Lo} and Q_{Lo} are the specified active and reactive powers of the load, respectively; k_f's denote the coefficients of the frequency characteristics of the load; k_v's are the coefficients of the voltage characteristics of the load; V and V_o are the actual and nominal voltage of the load bus; and f and f_o are the observed and nominal system frequency. As observed, the equations (1) and (2) represent simple models by which the load is linearly dependent with the frequency, while the voltage affects exponentially.

For generation buses, as well as traditional PV and PQ mode, the droop-control strategy is used for appropriate power sharing among DERs. For the droop-controlled DERs, the power equations vary with the utilized control strategy which are depending on their output impedance. In the case where the imaginary part of equivalent impedance is greater that the real part, the inductive droop mode is utilized. This strategy is often

called conventional droop mode, as the majority of inverter-interfaced DERs with their output filters meet this situation. By this strategy, the injected active and reactive powers are related to the frequency and voltage, respectively (i.e., $P_{Gi} = P_{Gi(f)}$ and $Q_{Gi} = Q_{Gi(V_i)}$). In contrast, when a resistive (or inverse) droop mode is enabled, active and reactive powers are related to the voltage and frequency, respectively (i.e., $P_{Gi} = P_{Gi(V_i)}$ and $Q_{Gi} = Q_{Gi(f)}$). While in the case of complex droop mode the active and reactive powers are related to both frequency and voltage (i.e., $P_{Gi} = P_{Gi(f,V_i)}$ and $Q_{Gi} = Q_{Gi(f,V_i)}$). Employing two binary parameters *x* and *y* makes it possible to express all three-droop operating mode in the unified formulas, as follows

$$P_{Gi(f,V_i)} = P_{G0i} - \left(\frac{x_i}{x_i+y_i}\right) \cdot \left(\frac{f-f_0}{m_i}\right) - \left(\frac{y_i}{x_i+y_i}\right) \cdot \left(\frac{V_i-V_{0i}}{n_i}\right) \tag{3}$$

$$Q_{Gi(f,V_i)} = Q_{G0i} + \left(\frac{y_i}{x_i+y_i}\right) \cdot \left(\frac{f-f_0}{m_i}\right) - \left(\frac{x_i}{x_i+y_i}\right) \cdot \left(\frac{V_i-V_{0i}}{n_i}\right) \tag{4}$$

$$\begin{cases} P_{Gi,min} \le P_{Gi} \le P_{Gi,max} \\ Q_{Gi,min} \le Q_{Gi} \le Q_{Gi,max} \end{cases} \tag{5}$$

where P_G/Q_G and P_{G0}/Q_{G0} are the injected and set-point active/reactive power, respectively; f_0 and V_0 are the frequency and voltage set-points, respectively; and m and n stand for the static frequency and voltage droop gains of the corresponding DER, respectively. The set of constraints (5) imposes bounds on the injections from the DERs. P_{G0} and Q_{G0} are normally set to zero and the operational requirements can be met by adjusting f_0 and V_0 [20]. By setting $x_i = 1$ and $y_i = 0$, one activates the conventional droop; whereas $x_i = 0$ and $y_i = 1$ expresses the inverse droop; and $x_i = 1$ and $y_i = 1$ enables the complex droop mode.

In conventional and PF-IMGs analysis, the network (branches and transformers) are represented by their nominal admittance that are drawn in the well-known $\boldsymbol{Y}_{bus}$ matrix. Since the frequency is a variable in the PF-IMGs, contrary to the traditional PF, the elements of $\boldsymbol{Y}_{bus}$ and consequently their partial derivations with respect to the frequency are not constant. In addition, no slack bus is included and any change in local power generation and/or demand would affect the system frequency [7]. With these considerations, the PF-IMGs mismatch equations are stated as follows

$$\begin{cases} \Delta P_{i(f,\boldsymbol{V},\boldsymbol{\delta})} = \sum_{j=1}^{j=N_b} \{V_i \cdot V_j \cdot Y_{ij(f)} \cdot \cos(\delta_i - \delta_j - \theta_{ij(f)})\} - [P_{Gi(f,V_i)} - P_{Li(f,V_i)}] \\ \Delta Q_{i(f,\boldsymbol{V},\boldsymbol{\delta})} = \sum_{j=1}^{j=N_b} \{V_i \cdot V_j \cdot Y_{ij(f)} \cdot \sin(\delta_i - \delta_j - \theta_{ij(f)})\} - [Q_{Gi(f,V_i)} - Q_{Li(f,V_i)}] \end{cases} \tag{6}$$

where N_b is the total number of buses; $Y_{ij}\angle\theta_{ij} \in \mathbb{C}$ is the ij^{th} element of the admittance matrix; and $V_i\angle\delta_i \in \mathbb{C}$ is the complex voltage at i^{th} bus. The main difference of the equations above compared to traditional PF equations is the inclusion of the system frequency as a variable. This dependency is also clearly stated in the elements of the admittance matrix and power injections, as previously discussed. After some mathematical manipulations, the PF iterative solution based on the NR can be finally cast in a matrix form as

$$\boldsymbol{x}^{(k+1)} = \boldsymbol{x}^{(k)} - \left[\mathbf{g}'\left(\boldsymbol{x}^{(k)}\right)\right]^{-1} \cdot \mathbf{g}\left(\boldsymbol{x}^{(k)}\right) \tag{7}$$

where $\mathbf{g}: \mathbb{R}^n \longmapsto \mathbb{R}^n$ are the PF equations (6); $[\cdot]^{-1}: \mathbb{R}^{n\times n} \mapsto \mathbb{R}^{n\times n}$ is the inverse operator; $\mathbf{g}' \in \mathbb{R}^{n\times n}$ is the Jacobian matrix formed by the first partial derivatives of (6) w.r.t. the variables; and $\boldsymbol{x} \in \mathbb{R}^n$ is the state vector which is defined as

$$\boldsymbol{x} = [f, \boldsymbol{\delta}, \boldsymbol{V}]^{\intercal} \tag{8}$$

where $\boldsymbol{\delta}$ and $\boldsymbol{V}$ are the vector of nodal voltage angles and magnitudes, respectively. It is worth noting that in contrast to the conventional PF, in which a slack bus with pre-specified voltage magnitude and angle is always fixed, here a Reference Bus (RB) with only pre-specified δ (normally zero) is considered and its voltage magnitude is included in $\boldsymbol{V}$. Furthermore, in addition to traditional flat start initial guesses (i.e., $\boldsymbol{\delta} = 0$ and $\boldsymbol{V} = 1$), the initial operating condition for variable system frequency, f, is set to f_0, while V_i for buses with droop-controlled DERs is set to V_{0i}. Concisely, compared to conventional PF, the mismatch equations for RB is also considered to handle two extra states namely f and V_{RB}.

3 - The developed HOMMP for PF-IMGs

3.1 - Outlines of the MMP for solving set of ordinary differential equations (ODEs)

In this section, the MMP for solving set of ordinary ODEs is firstly described. It supposes the original use of this technique, and the developed solver has been built based on the formulation below. Let us consider a set of n ODEs, as follows:

$$\dot{\boldsymbol{y}}(t) = \boldsymbol{\varphi}\big(\boldsymbol{y}(t)\big) \tag{9}$$

where, $\dot{\boldsymbol{y}}(t) = \nabla_t \boldsymbol{y}(t)$ is the system vector, $\boldsymbol{\varphi}: \mathbb{R}^n \mapsto \mathbb{R}^n$ and t is usually the time. Considering an initial time instant t_0 and H step size (or time step), the MMP starts evaluating (9) for N intermediate points as follows

$$\begin{cases} \dot{\boldsymbol{y}}(t_0) = \boldsymbol{\varphi}\big(\boldsymbol{y}(t_0)\big) \\ \dot{\boldsymbol{y}}(t_1) = \dot{\boldsymbol{y}}(t_0) + h \cdot \boldsymbol{\varphi}\big(\boldsymbol{y}(t_0)\big) \\ \dot{\boldsymbol{y}}(t_2) = \dot{\boldsymbol{y}}(t_1) + 2 \cdot h \cdot \boldsymbol{\varphi}\big(\boldsymbol{y}(t_1)\big) \\ \quad \vdots \\ \dot{\boldsymbol{y}}(t_{i+1}) = \dot{\boldsymbol{y}}(t_{i-1}) + 2 \cdot h \cdot \boldsymbol{\varphi}\big(\boldsymbol{y}(t_i)\big) \end{cases} \tag{10}$$

where, $h = H/N$. As seen, the first step ($i = 1$) is calculated using the Euler method, whereas for remainder points, the ODEs are evaluated using a double grid namely $2h$ and the $(i-1)^{th}$ calculated point. Therefore, the MMP requires to evaluate the concerned function N times. In the solution of ODEs, the parameter N is normally taken variable, being adapted according the requirements of the system to keep the error properly bounded. Finally, the system vector is updated using the trick introduced by Gragg [24], as follows

$$\dot{\boldsymbol{y}}(t_0 + H) = \frac{1}{2} \cdot \big[\dot{\boldsymbol{y}}(t_N) + \dot{\boldsymbol{y}}(t_{N-1}) + h \cdot \boldsymbol{\varphi}\big(\boldsymbol{y}(t_N)\big)\big] \tag{11}$$

The trick (11) was introduced to avoid large and sustained oscillations around a constant value. In the following subsection, the iterative multi-step scheme (9)-(11) dedicated to ODEs is adapted for solution of system of nonlinear equations, resulting in a solver with $(N+1)^{th}$ order of convergence.

3.2 - The developed PF-IMGs solver

Let us begin observing the first step of (10) which, as said before, corresponds to the conventional Euler's procedure. In [25] was shown that the NR can be conceived as the application of the Euler's technique to PF problem. Applying the same principle, the HOMMP begins calculating a first intermediate point, namely $\boldsymbol{x}_1$, using the NR as follows

$$\boldsymbol{x}_0^{(k)} = \boldsymbol{x}^{(k)} \tag{12}$$

$$\boldsymbol{x}_1^{(k)} = \boldsymbol{x}_0^{(k)} - \alpha_1 \cdot \left[\mathbf{g}'\left(\boldsymbol{x}_0^{(k)}\right)\right]^{-1} \cdot \mathbf{g}\left(\boldsymbol{x}_0^{(k)}\right) \tag{13}$$

where $\alpha_1 \in \mathbb{R}$ replaces the step size h and will be tuned to achieve higher convergence rate (see Section 3.C). The assimilation of the Euler as a conventional NR mapping is based on a clear analogy between these two methods. Indeed, one can easily deduce an analogy between the mapping (9) and (13) if the function $\boldsymbol{\varphi}$ is replaced by $\boldsymbol{x} - [\mathbf{g}'(\boldsymbol{x})]^{-1}\mathbf{g}(\boldsymbol{x})$, as Milano deduced in [25]. This idea allows to adapt the MMP procedure (10) to systems of nonlinear equations in the same way (PF-IMGs in our particular case). However, if the similitude between the Euler and NR methods is directly applied to (10), the resulting iterative algorithm would be computationally costly due to the Jacobian matrix should be evaluated and factorized N times as $\boldsymbol{\varphi}$ is in turn evaluated at N different points. Since this calculation supposes the heaviest part of any Newton-like method [25], it is necessary to reduce the number of factorizations to obtain a competitive solver. In this sense, we adduce to the structure of the well-known multistep (or multipoint) nonlinear solvers [21]. This kind of methods achieve high convergence rate by evaluating the function at several points rather than the Jacobian. In fact, if one examines e.g. [21, eq. (2)], which corresponds with a generic multistep nonlinear solver, a clear analogy is observed with the method (10). In this case, the function $\boldsymbol{\varphi}$ should be replaced by $\boldsymbol{\Phi}$, which is defined for convenience as follows

$$\boldsymbol{\Phi}(\boldsymbol{v}, \boldsymbol{w}, \boldsymbol{z}) = [\mathbf{g}'(\boldsymbol{v})]^{-1} \cdot [\mathbf{g}(\boldsymbol{w}) + \mathbf{g}(\boldsymbol{z})] \tag{14}$$

where $\boldsymbol{v}, \boldsymbol{w}, \boldsymbol{z} \in \mathbb{R}^n$ are arbitrary vectors. The function (14) is particularly important for the new proposal since allows to reuse the LU decomposition calculated at $\boldsymbol{v}$. Thereby, the Jacobian and the function $\mathbf{g}$ can be evaluated at different points, thus avoiding to compute extra Jacobian factorizations, which are, by far, the heaviest calculation in Newton-like methods [21]. Once the function (14) is defined, the ideas outlined in [25] and the multistep nonlinear paradigm drawn in [21, eq. (2)] can be combined to obtain a multistep PF-IMGs solver defined as

$$\begin{cases} \boldsymbol{x}_2^{(k)} = \boldsymbol{x}_0^{(k)} - 2 \cdot \alpha_2 \cdot \boldsymbol{\Phi}\left(\boldsymbol{x}_0^{(k)}, \boldsymbol{x}_0^{(k)}, \boldsymbol{x}_1^{(k)}\right) \\ \boldsymbol{x}_3^{(k)} = \boldsymbol{x}_1^{(k)} - 2 \cdot \alpha_3 \cdot \boldsymbol{\Phi}\left(\boldsymbol{x}_0^{(k)}, \boldsymbol{x}_1^{(k)}, \boldsymbol{x}_2^{(k)}\right) \\ \quad \vdots \\ \boldsymbol{x}_N^{(k)} = \boldsymbol{x}_{N-2}^{(k)} - 2 \cdot \alpha_N \cdot \boldsymbol{\Phi}\left(\boldsymbol{x}_0^{(k)}, \boldsymbol{x}_{N-2}^{(k)}, \boldsymbol{x}_{N-1}^{(k)}\right) \end{cases} \tag{15}$$

$$\boldsymbol{x}^{(k+1)} = \frac{1}{2} \cdot \left[\boldsymbol{x}_N^{(k)} + \boldsymbol{x}_{N-2}^{(k)} - \beta \cdot \boldsymbol{\Phi}\left(\boldsymbol{x}_0^{(k)}, \boldsymbol{x}_{N-2}^{(k)}, \boldsymbol{x}_{N-1}^{(k)}\right)\right] \tag{16}$$

where α's, $\beta \in \mathbb{R}$ are tuned to achieve high convergence order (see Section 3.C). The mapping (13)-(16) supposes the main core of the developed HOMMP in which α's, β

and N are parameters whose importance is posteriorly discussed. The developed HOMMP responds to the standard multistep (or multipoint) structure in which the Jacobian matrix is only factorized (and evaluated) once per iteration. Indeed, as observed in (16), the function $\boldsymbol{\Phi}$ takes $\boldsymbol{x}_0^{(k)}$ for the Jacobian calculation. Therefore, if one observes (14), it can be deduced that the Jacobian must be factorized once each iteration, resulting in a computational burden similar to the NR. Certainly, HOMMP involves more function evaluations and linear systems solutions than NR, nevertheless, these calculations can be efficiently addressed and they do not have a significant impact in the overall computational cost [25].

For the sake of summarizing, Table 1 collects the main calculations involved in the developed HOMMP. It is also worth noting that the solution of $\mathbf{g}$ is a type-0 fixed point of the mapping (13)-(16), therefore, the developed HOMMP constitutes an asymptotically stable PF-IMGs solver. These proofs are trivial, and they have not been included for simplicity, being referred to [25] for a further explanation.

Table 1 - Main calculations involved in the developed HOMMP

Calculation	Required each iteration
LU decompositions	1
Function evaluations	N
Linear systems	N
Matrix systems	0

3.3 - Convergence analysis of the developed HOMMP

It remains to be studied the convergence order of the developed HOMMP. So far, we have demonstrated that computationally cost of the developed solver is similar to NR as the Jacobian matrix is factorized once each iteration. However, if the order of convergence is less than or equal to two, the resulting algorithm would be not competitive with the conventional NR. In this regard, the Theorem 1 is devoted on proving the $(N+1)^{th}$ order of convergence of the developed HOMMP technique. To this end, the Taylor expansion technique [21] has been used.

Theorem 1. Let $\mathbf{g}$: D $\subseteq \mathbb{R}^n \mapsto \mathbb{R}^n$ be sufficiently differentiable at each point of an open neighborhood D of $\boldsymbol{r} \in \mathbb{R}^n$, this is a solution of the system $\mathbf{g}(\boldsymbol{x}) = \mathbf{0}$. Let us suppose that $\mathbf{g}(\boldsymbol{x})$ is continuous and nonsingular in $\boldsymbol{x}$. Then, the sequence $\{\boldsymbol{x}^{(k)}\}_{k\geq 0}$ obtained using the developed HOMMP converges to $\boldsymbol{r}$ with order $N+1$ if and only if $\alpha_1 = \beta = 1$ and $\alpha_i = \frac{1}{2};\ \forall i \in \{2,3,\dots,N\}$

Proof. From the Taylor expansion of $\mathbf{g}(\boldsymbol{x}^{(k)})$ and $\mathbf{g}'(\boldsymbol{x}^{(k)})$ about $\boldsymbol{r}$, we obtain

$$\mathbf{g}\left(\boldsymbol{x}_0^{(k)}\right) = \mathbf{g}'(\boldsymbol{r}) \cdot \left[\boldsymbol{e}^{(k)} + \boldsymbol{C_2} \cdot \boldsymbol{e}^{(k)^2} + \boldsymbol{C_3} \cdot \boldsymbol{e}^{(k)^3}\right] + \boldsymbol{O}\left(\boldsymbol{e}^{(k)^4}\right) \tag{17}$$

$$\mathbf{g}'\left(\boldsymbol{x}_0^{(k)}\right) = \mathbf{g}'(\boldsymbol{r}) \cdot \left[\boldsymbol{I} + 2 \cdot \boldsymbol{C_2} \cdot \boldsymbol{e}^{(k)} + 3\boldsymbol{C_3} \cdot \boldsymbol{e}^{(k)^2}\right] + \boldsymbol{O}\left(\boldsymbol{e}^{(k)^3}\right) \tag{18}$$

where $\boldsymbol{e}^{(k)} = \boldsymbol{x}^{(k)} - \boldsymbol{r} \in \mathbb{R}^n$, $\boldsymbol{e}^i = \underbrace{(\boldsymbol{e}, \boldsymbol{e}, \dots, \boldsymbol{e})}_{i-\text{times}}$, $\boldsymbol{C}_j = (1/j!)[\mathbf{g}'(\boldsymbol{r})]^{-1}\mathbf{g}^{(j)}(\boldsymbol{r}) \in L_i(\mathbb{R}^n, \mathbb{R}^n)$, $\mathbf{g}^{(j)} \in L(\mathbb{R}^n \times \dots \times \mathbb{R}^n, \mathbb{R}^n)$, $[\mathbf{g}'(\boldsymbol{r})]^{-1} \in L(\mathbb{R}^n)$ and $\boldsymbol{I} \in \mathbb{R}^{n\times n}$ is the identity matrix. The inversion of (18) can be calculated through the inverse definition. For the sake of brevity, let us provide here just the result, being referred to [5] for a further explanation

$$\left[\mathbf{g}'\left(\boldsymbol{x}_0^{(k)}\right)\right]^{-1} = \left[\boldsymbol{I} - \boldsymbol{X_1}\cdot\boldsymbol{e}^{(k)} + \boldsymbol{X_2}\cdot\boldsymbol{e}^{(k)^2} - \boldsymbol{X_3}\cdot\boldsymbol{e}^{(k)^3}\right]\cdot[\mathbf{g}'(\boldsymbol{r})]^{-1} + \boldsymbol{O}\left(\boldsymbol{e}^{(k)^4}\right) \tag{19}$$

where $\boldsymbol{X_1} = 2\cdot\boldsymbol{C_2}$, $\boldsymbol{X_2} = (4\cdot\boldsymbol{C_2^2} - 3\boldsymbol{C_3})$ and $\boldsymbol{X_3} = (4\cdot\boldsymbol{C_4} - 12\cdot\boldsymbol{C_2}\cdot\boldsymbol{C_3} + 8\cdot\boldsymbol{C_2^3})$. It is noteworthy that only three terms of the inverse function were calculated, nevertheless, infinity terms could be calculated easily following the same procedure. However, it lacks of sense for the present deduction. Substituting (17) and (19) into (13) yields

$$\boldsymbol{e}_1^{(k)} = \boldsymbol{x}_0^{(k)} - \alpha_1\cdot\left[\mathbf{g}'\left(\boldsymbol{x}_0^{(k)}\right)\right]^{-1}\cdot\mathbf{g}\left(\boldsymbol{x}_0^{(k)}\right) - \boldsymbol{r} = (\boldsymbol{C_3} - \boldsymbol{C_2^2})2\cdot\alpha_1\cdot\boldsymbol{e}^{(k)^3} + \alpha_1\cdot\boldsymbol{C_2}\cdot \boldsymbol{e}^{(k)^2} + (1-\alpha_1)\cdot\boldsymbol{e}^{(k)} + \boldsymbol{O}\left(\boldsymbol{e}^{(k)^4}\right) \tag{20}$$

where $\boldsymbol{e}_j^{(k)} = \boldsymbol{x}_j^{(k)} - \boldsymbol{r}$. As seen in (20), the procedure (13) yields linear convergence because the term $\boldsymbol{e}^{(k)}$ has not vanished. Nevertheless, the developed procedure is sufficiently versatile to eliminate it if the parameter α_1 is properly tuned. Indeed, by observing (20) it can be easily deduced that quadratic convergence is only possible if $\alpha_1 = 1$, which yields

$$\boldsymbol{e}_1^{(k)}\Big|_{\alpha_1=1} = \boldsymbol{C_2}\cdot\boldsymbol{e}^{(k)^2} + \boldsymbol{O}\left(\boldsymbol{e}^{(k)^3}\right) \tag{21}$$

As seen, the parameter α_1 allows to eliminate $\boldsymbol{e}^{(k)}$ in (20) and thus achieving superior convergence. Nevertheless, the deduction so far does not contribute with any novelty as the resulting map corresponds with the conventional NR, which was expected since the first step of the developed method was assimilated to the Newton's technique, as discussed before. To achieve higher convergence rate, the other steps in (15) play a crucial role. To analyze them, let us define the Taylor expansion of $\boldsymbol{\Phi}$ about $\boldsymbol{r}$ as

$$\boldsymbol{\Phi}\left(\boldsymbol{x}_0^{(k)}, \boldsymbol{x}_{j-2}^{(k)}, \boldsymbol{x}_{j-1}^{(k)}\right) = \left[\boldsymbol{I} - \boldsymbol{X_1}\cdot\boldsymbol{e}^{(k)} + \boldsymbol{X_2}\cdot\boldsymbol{e}^{(k)^2} - \boldsymbol{X_3}\cdot\boldsymbol{e}^{(k)^3}\right]\cdot\left[\left(\boldsymbol{e}_{j-1}^{(k)} + \boldsymbol{e}_{j-2}^{(k)}\right) + \boldsymbol{C_2}\cdot \left(\boldsymbol{e}_{j-1}^{(k)\,2} + \boldsymbol{e}_{j-2}^{(k)\,2}\right) + \boldsymbol{C_3}\cdot\left(\boldsymbol{e}_{j-1}^{(k)\,3} + \boldsymbol{e}_{j-2}^{(k)\,3}\right)\right] = \boldsymbol{e}_{j-2}^{(k)} + \boldsymbol{e}_{j-1}^{(k)} + \boldsymbol{C_2}\cdot\boldsymbol{e}_{j-2}^{(k)\,2} + \boldsymbol{C_2}\cdot\boldsymbol{e}_{j-1}^{(k)\,2} + \dots \tag{22}$$

It is noteworthy to note that $\boldsymbol{e}_{j-2}^{(k)}$ upper bounds the convergence order of (22). So that, the Taylor expansion (22) could be trivially simplified by

$$\boldsymbol{\Phi}\left(\boldsymbol{x}_0^{(k)}, \boldsymbol{x}_{j-2}^{(k)}, \boldsymbol{x}_{j-1}^{(k)}\right) = \boldsymbol{e}_{j-2}^{(k)} + \boldsymbol{O}\left(\boldsymbol{e}_{j-1}^{(k)}\right) \tag{23}$$

The expression (23) establishes that the order of convergence for the j^{th} of the developed method is in fact bounded by the $(j-2)^{th}$ step, which results inefficient. To solve this issue, we make use of (23), from which the generic error function for the j^{th} step of the mapping (15) can be derived as

$$\boldsymbol{e}_j^{(k)} = \boldsymbol{e}_{j-2}^{(k)} - 2\alpha_j \boldsymbol{\Phi}\left(\boldsymbol{x}_0^{(k)}, \boldsymbol{x}_{j-2}^{(k)}, \boldsymbol{x}_{j-1}^{(k)}\right) = \boldsymbol{e}_{j-2}^{(k)} - 2 \cdot \alpha_j \cdot \boldsymbol{e}_{j-2}^{(k)} + \boldsymbol{O}\left(\boldsymbol{e}_{j-1}^{(k)}\right); j \geq 2 \tag{24}$$

The equation (24) reflects the importance of the α's parameters. In fact, the order of convergence can be increased by properly tuning them. In this case, it is clear than the maximum order of convergence in (24) is achieved with $\alpha_j = \frac{1}{2}$, for which the term $\boldsymbol{e}_{j-2}^{(k)}$ vanishes. It is noteworthy that the expression (24) is valid for any $j \geq 2$. Therefore, the parameter α should be tuned equal to $\frac{1}{2}$ regardless the step counter. With this adoption, the error function for all the steps involved in (15) can be calculated, yielding

$$\begin{cases} \boldsymbol{e}_2^{(k)} = 2 \cdot \boldsymbol{C_2^2} \cdot \boldsymbol{e}^{(k)^3} + \boldsymbol{O}\left(\boldsymbol{e}^{(k)^4}\right) \\ \boldsymbol{e}_3^{(k)} = 4 \cdot \boldsymbol{C_2^3} \cdot \boldsymbol{e}^{(k)^4} + \boldsymbol{O}\left(\boldsymbol{e}^{(k)^5}\right) \\ \vdots \\ \boldsymbol{e}_j^{(k)} = 2^{j-1} \cdot \boldsymbol{C_2^j} \cdot \boldsymbol{e}^{(k)^{j+1}} + \boldsymbol{O}\left(\boldsymbol{e}^{(k)^{j+2}}\right) \\ \vdots \\ \boldsymbol{e}_N^{(k)} = 2^{N-1} \cdot \boldsymbol{C_2^N} \cdot \boldsymbol{e}^{(k)^{N+1}} + \boldsymbol{O}\left(\boldsymbol{e}^{(k)^{N+2}}\right) \end{cases} \tag{25}$$

The error function for the last step of the HOMMP (16) can be written by using the results obtained in (25), as follows

$$\underbrace{\boldsymbol{x}^{(k+1)} - \boldsymbol{r}}_{\boldsymbol{e}^{(k+1)}} = \frac{1}{2} \cdot \left[\boldsymbol{e}_N^{(k)} + \boldsymbol{e}_{N-2}^{(k)} - \beta \cdot \boldsymbol{\Phi}\left(\boldsymbol{x}_0^{(k)}, \boldsymbol{x}_{N-2}^{(k)}, \boldsymbol{x}_{N-1}^{(k)}\right)\right] \tag{26}$$

As demonstrated by (22), the order of convergence of the function $\boldsymbol{\Phi}\left(\boldsymbol{x}_0^{(k)}, \boldsymbol{x}_{N-2}^{(k)}, \boldsymbol{x}_{N-1}^{(k)}\right)$ would be $\boldsymbol{e}_{N-2}^{(k)}$. Keeping this in mind, it is clear that $\beta = 1$ would yield the maximum order of convergence in (26), since this adoption would eliminate the error $\boldsymbol{e}_{N-2}^{(k)}$. Thus, assuming $\beta = 1$, the expression (26) can be developed, yielding

$$\boldsymbol{e}^{(k+1)} = \frac{1}{4} \cdot 2^N \cdot \boldsymbol{C_2^N} \cdot \boldsymbol{e}^{(k)^{N+1}} + \boldsymbol{O}\left(\boldsymbol{e}^{(k)^{N+2}}\right) \tag{27}$$

The equation (27) stands for the error function at the $(k+1)^{th}$ iteration and, consequently, determines the order of convergence of the HOMMP [5]. Thereby, it has been proved that the developed HOMMP converges to $\boldsymbol{r}$ with order $N+1$ as maximum, which completes the proof. □

Theorem 1 is especially relevant since, besides demonstrating the order of convergence of the developed HOMMP, it deduces the ideal values for the α's and β. In this way, these parameters are not free since it lacks of sense giving them other different values. This result therefore simplifies the applicability of the developed solver, omitting the existence of free parameters that may be case-dependent, as occurred with other PF solvers (e.g. [25]).

3.4 - Computational comparison with other solvers

In this section, the computational cost of the developed HOMMP is compared with the conventional NR. The NR supposes the most conventional solver for PF problems in IMGs and transmission systems [25]. This way, it results useful comparing the developed solver with the Newton's technique. In addition, we have included the 6th order method

(6OM) developed in [26] for comparison. This technique demonstrated a good performance in large-scale transmission networks, and it can be easily adapted to IMGs. In [26], other two HONL solvers were developed, however, the 6OM turned out to be clearly superior. Therefore, it is reasonable including only the 6OM in the analysis.

From a computational point of view, two nonlinear solvers can be compared using the so-called efficiency index, which is defined as follows [7]

$$FEI = p^{1/CO} \tag{28}$$

where, p is the order of convergence and CO stands for the total computational cost of an iteration in terms of flops. In this sense, the following theorem is generally used to estimate the cost of a LU decomposition [27].

Theorem 2. The number of products and quotients required for solving q linear systems of equations with the same matrix of coefficients, by using LU factorization, is

$$o(n,q) = \frac{1}{3}n^3 + qn^2 - \frac{1}{3}n \tag{29}$$

Proof. See [26]. □

It is also necessary to consider the computational cost of each function evaluation $o(\mathbf{g})$ and Jacobian evaluation $o(\mathbf{g}')$. Thereby, the total computational cost of an iteration can be estimated as follows

$$CO = K_1 \cdot o(\mathbf{g}) + K_2 \cdot o(\mathbf{g}') + \sum_{j=1}^{j=N_{LU}} K_{3j} \cdot o\left(n, q_j\right) \tag{30}$$

where K_1, K_2 and K_3 stand for the total number of function evaluations, Jacobian evaluations and linear systems solutions with the same LU decomposition per iteration, respectively; and N_{LU} is the total number of LU decompositions each iteration. However, while (29) is suitable for small-scale systems, it is not fully indicative for large cases since it tends to 1 if n is high. Anyway, it can be still used for comparison purposes. The following theorem is devoted on calculating the efficiency index for the developed HOMMP.

Theorem 3. *For HOMMP, we have* $FEI = (N+1)^{\frac{1}{\frac{1}{3}n^3+(N+1)n^2+\frac{3N-1}{3}n}}$

Proof. The developed HOMMP requires N functions evaluation besides a Jacobian factorization each iteration. In addition, it requires to solve N linear systems using the same LU decomposition, consequently one has $CO = Nn + n^2 + \frac{1}{3}n^3 + Nn^2 - \frac{1}{3}n = \frac{1}{3}n^3 + (N+1)n^2 + \frac{3N-1}{3}n$ □

Fig. 1 compares the efficiency index (29) for the conventional NR, 6OM and HOMMP for various values of N. As observed, the developed solver outperforms NR and 6OM for $N \geq 2$. This is expected since the HOMMP presents higher convergence rate than NR, while each iteration is maintained computationally light as just one LU decomposition is required. On the other hand, the 6OM requires two Jacobian evaluations and factorizations per iteration, which serves to outperform NR but not HOMMP. It is worth noting that no further improvement is observed beyond $N = 4$, this is due to the

increment of the convergence order does not compensate the extra Jacobian and function evaluations required. Therefore, by the analysis performed in this section, it seems clear that $N > 4$ is not justified. As empirically demonstrated in Section 4, the ideal value for N is normally between 3 or 4. Nevertheless, the developed method turns out to be well-behaved with both values and, therefore, it can be set coarsely without any problem.

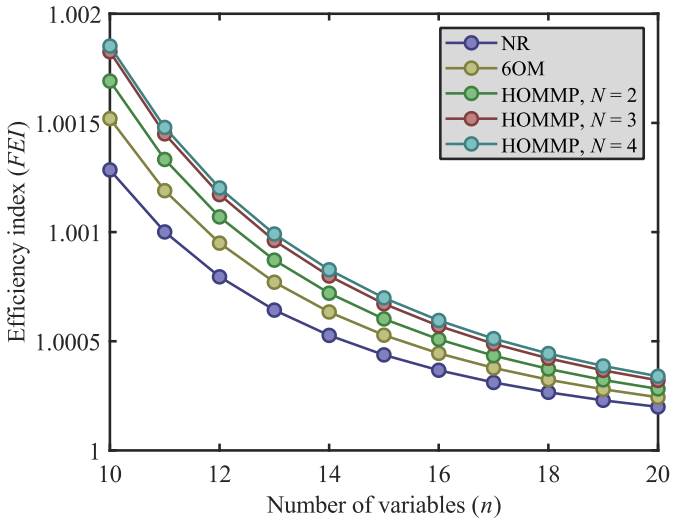

Figure 1 - Comparison of the efficiency index (28) for the NR, 6OM and HOMMP for different values of N

3.5 - Computational implementation

Industrial software packages usually incorporate the NR code by default since, as commented, this solver is by far the most conventional one and has been widely used in a variety of tools. Some available nonlinear solvers are hard to be implemented because they require major modifications of standard codes. This is the case, for example, of the 2nd order solvers [28], which requires to implement a secondary routine for the calculation of the Hessian, or the optimal multiplier-based techniques [29], which needs a subroutine for optimally calculating the step size iteratively. In this regard, Fig. 2 presents the flowcharts of the NR, the loop-based method [14, 20] and the developed HOMMP solver as applied to PF-IMGs. As seen in this figure, the overall procedure of the HOMMP is quite similar to that implemented for other standard solvers. Actually, only the so-called Modified midpoint loop has to be added. This routine however does not entail extra calculations, since it only needs the Jacobian matrix and the values of α's, β and N as entries. For these steps, the computational processes already implemented to calculate the Jacobian and PF equations can be reused, thus saving codification efforts. This structure allows to easily reuse available codes for the NR. In this way, the implementation of the HOMMP in commercial software tools is straightforward, requiring only some minor modifications.

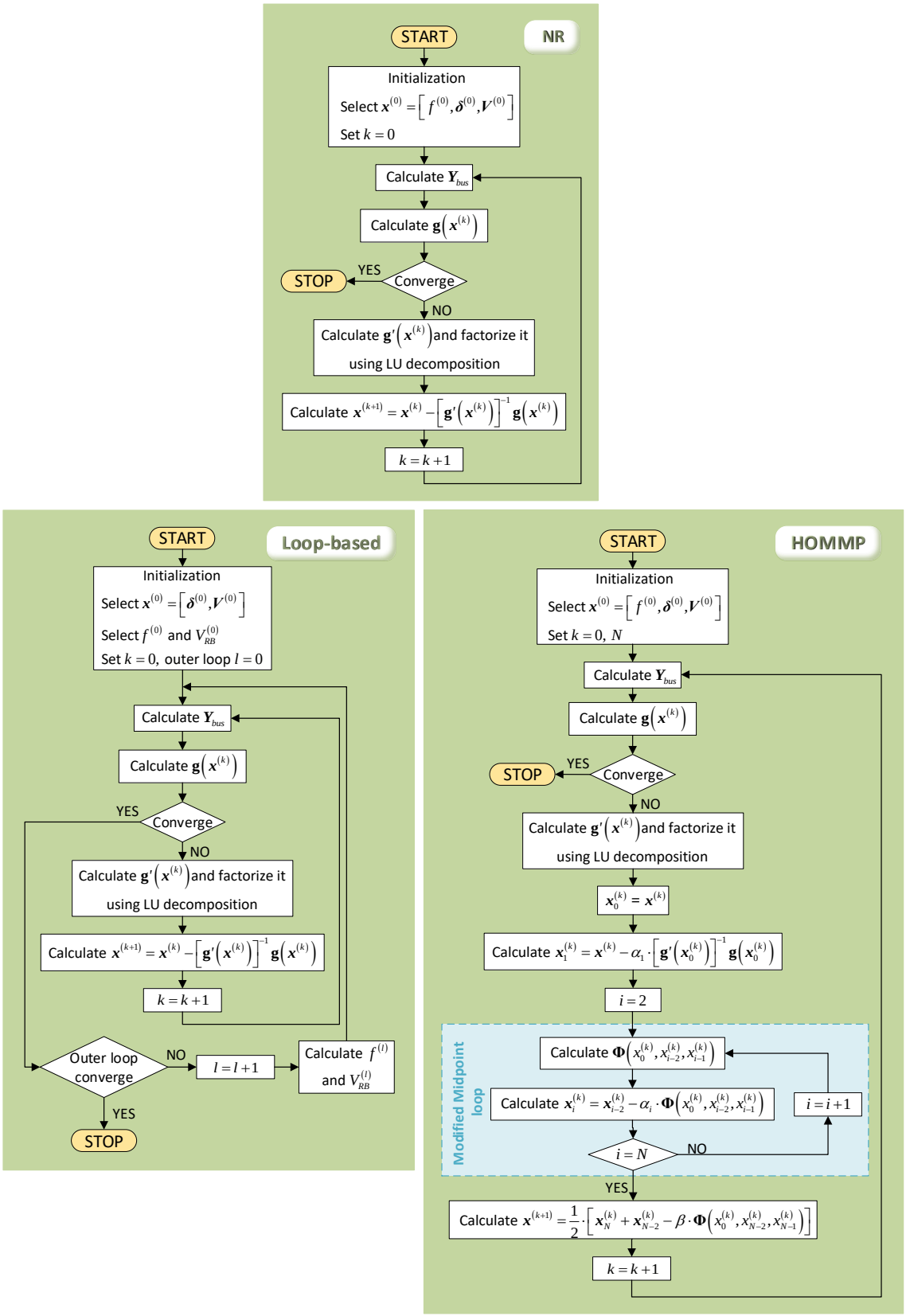

Figure 2 - Flowcharts of the NR, Loop-based solvers and HOMMP as applied to PF-IMGs

3.6 - Limitations

A priori, the developed solver does not present any important limitation beyond those showed by NR and other derived techniques. Therefore, it can be straightforward applied

to any network and system in which NR can be used as well. In this regard, maybe the main barrier of the developed method is its applicability in ill-conditioned systems. As pointed out in [25], ill-conditioned systems are characterized for provoking divergence of NR, which is naturally caused by a badly-initialization. In this sense, a flat starter may lie far away to the final solution, and at last out of the so-called region of attraction of NR, which causes divergence. The behavior of high-order Newton-like methods in ill-conditioned cases is still very few studied, however, some studies pointed out that high order methods may be weaker than NR in ill-conditioned cases [30]. Nevertheless, ill-conditioned cases mainly appear in very large-scale systems (>3,000 buses), which is an unusual situation for IMGs. Therefore, the new proposal is presumably straightforward applicable to a wide variety of cases, configurations and load profiles that may appear in IMG operation without any important limitation.

4 - Numerical Experiments

In this section, the proposed HOMMP method is compared with the NR method and 6OM method in 10 different IMGs. Different topologies (i.e., radial or weakly meshed), different load models and different droop control strategies are considered to have a comprehensive study. The main features of the studied test systems are reported in Table 2. To validate the PF-IMGs results it is vital to compare the results with the steady-state values obtained from time-domain simulations. This issue is reasonable and feasible to perform for small-scale systems, which is performed for systems #1 to #6. The results for all studied methods are consistent with high accuracy compared to the steady-state results obtained by PLECS software. Consequently, the accuracy of the results obtained for other test systems has been accepted. Three different scenarios namely base-case, increased load level, and increased R/X ratio are investigated. For the first scenario, different convergence tolerances ε are imposed, while for the rest $\varepsilon = 10^{-6}$ has been taken. The flat start (i.e., $\boldsymbol{V} = 1$ p.u., $\boldsymbol{\delta} = 0$, and $f = 1$ p.u.) is considered as an initial solution for all methods, except for $\boldsymbol{V}$ of the droop-controlled buses and f, which depends on operational settings and might be varied. All the tested methodologies were coded under Matlab environment using the Matpower software package [31]. All simulations have been run under Windows 10 on a 2.0-2.6 GHz Intel Core i7-4510U personal laptop (8 GB RAM). In addition, the reported computational times have been obtained as the mean value of 5000 simulations, in order to minimize the influence of other computational activities.

Table 2 - Main features of the studied test systems

Sys. No.	Name	Branches No.	DERs No.	DERs Capacity (MW)	DERs Capacity (MVar)	Nominal Load (MW)	Nominal Load (MVar)	Voltage (kV)	Freq. (Hz)	DERs Droop Mode	Load Model	Reference
#1	The 7-bus system-case1	6	3	0.020	0.012	0.010	0.003	0.40	50	All CD	M: CP, CZ	[20]
#2	The 7-bus sysrem-case2									All ID	M: CP, CZ	[20]
#3	The 7-bus system-case3									All COD	M: CP, CZ	[20]
#4	The 7-bus system-case4									M: CD, PV	M: CP, CZ	[20] WM
#5	The 38-bus system-case1	37	5	6.55	3.00	3.71	2.30	12.66	60	All CD	M: R, I, C	[8]
#6	The 38-bus system-case2									All CD	M: R, I, C	[8] WM
#7	The 41-bus system	40	14	0.890	0.552	0.687	0.284	0.40	50	All CD	M: R, I, C	[32] WM, [20]
#8	The 69-bus system	68	5	7.80	4.83	3.80	2.70	12.66	60	All CD	CP	[33] WM
#9	The 118-bus system-case1	132	6	44.00	27.27	22.71	17.00	11.00	NS	All CD	CP	[34] WM
#10	The 118-bus system-case2									All CD	M: CP, R, I, C	

CB: Capacitor Bank, CD: Conventional Droop, ID: Inversed Droop, COD: Complex Droop, CP: Constant Power, CZ, Constant Impedance, R: Residential, I: Industrial, C: Commercial, M: Mixed, WM: With Modifications, NS: Not Specified. Note: In System #4 a capacitor with the capacity of 500 Var at nominal voltage and nominal frequency is placed at bus 7. In System #6 compared to System # 5, in addition to the different load coefficients, capacitor effect of some lines is considered.

4.1 - Base-case scenario

In this section, in order to verify the results of the proposed method and its superiority in the ability to solve systems with different sizes and conditions, in addition to comparing the NR and 6OM results, the results of loop-based methods with 1 loop (1L), 2 loops (2L), and 3 loops (3L) are also presented. First, the results have been reported in terms of the total number of iterations/repetitions for two different convergence criteria, in Table 3. The developed HOMMP method under the studied schemes N = 2, 3 and 4 presents third, fourth and fifth convergence rate, respectively. As can be seen, this characteristic allows to the developed algorithm converges in fewer iterations than the NR and 6OM methods. It is worth noting that in the theoretical papers, base-case scenario normally corresponds to the hypothetic situation in which the generators can deliver as much reactive power as the system demands. However, in this paper to attain logical results in accordance with the electrical conditions of the system, in the base-case, as well as other scenarios, both active and reactive limitations of DERs are considered according to (5). Exposure to these conditions in the Systems #5, #6, #8 and #9 has influenced the number of iterations. This issue is further investigated in the following subsection. Besides, the relatively large number of DERs in System #7 has led to an increase in the number of iterations. Referring to Table 3, some explanations and discussion can be found on loop-based methods. In these cases, the presented values refer to the total number of outer loops for calculating the f and V_{RB}. The 2L and 3L methods, consist of 2 and 3 nested loops, respectively, in which several conventional PF analyses (e.g., the NR) is performed, the numbers in brackets refers to the total number of conventional PF analysis. Method 1L can handle all types of droop modes and is computationally efficient in most cases. Method 3L is complementary to Method 2L for large-scale systems, as stated in [14]. However, methods 1L and 2L in some cases diverge with the format presented in the [20] and [14], indicating require modifications in the procedure of f and V_{RB} adjustment. Generally, the loop-based methods, take more computational time compared to the NR, 6OM and HOMMP methods, due to their repetitive nature. It is also deduced from Table 3 that performance of the developed HOMMP method in all schemes are less affected by increasing the convergence tolerance. To have an in-depth insight on convergence process, the convergence characteristics of the Systems #5 and #10 are plotted in Fig. 3.

Table 3 - Comparison of the Total Number of Iterations/Repetitions at Base-case Scenario

Syst. No.	$\varepsilon = 10^{-6}$								$\varepsilon = 10^{-8}$							
	NR	6OM	HOMMP			Loop-based methods			NR	6OM	HOMMP			Loop-based methods		
			N = 2	N = 3	N = 4	1L	2L	3L			N = 2	N = 3	N = 4	1L	2L	3L
#1	6	3	3	2	2	7 (7)	18 (56)	18 (68)	8	4	4	3	2	7 (7)	18 (56)	18 (68)
#2	7	4	4	3	2	46 (46)	US	US	10	5	5	3	3	46 (46)	US	US
#3	8	4	4	3	2	18 (18)	US	US	11	6	6	4	3	18 (18)	US	US
#4	4	2	2	2	1	7 (7)	16 (52)	19 (79)	6	3	3	2	2	7 (7)	16 (52)	19 (79)
#5	11	6	6	4	3	*	*	28(223)	15	8	8	6	4	*	*	28(223)
#6	13	7	7	5	4	*	*	25(128)	17	9	9	6	5	*	*	25(128)
#7	18	9	9	6	5	50(50)	*	20(111)	24	12	12	8	6	50(50)	*	20(111)
#8	12	6	6	4	3	22(22)	16(37)	18(78)	17	8	9	6	5	22(22)	16(37)	18(78)
#9	15	7	8	6	4	*	*	21(119)	20	10	10	7	6	*	*	21(119)
#10	12	6	6	4	4	*	*	21(124)	17	9	9	6	5	*	*	21(124)

*: Diverged, US: Unable to Solve

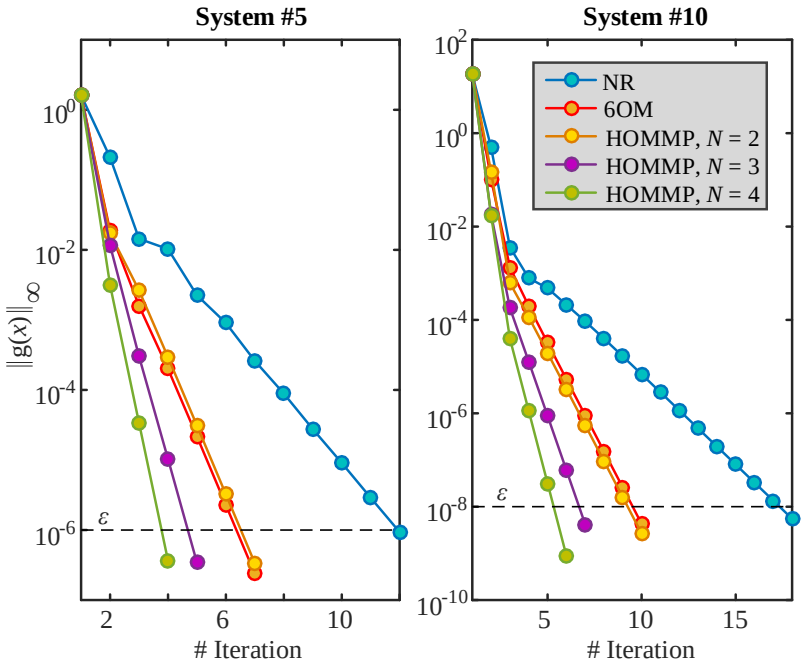

Figure 3 - Convergence characteristics of the System #5 (for $\varepsilon = 10^{-6}$) and System #10 (for $\varepsilon = 10^{-8}$) at base-case scenario.

Table 4 reports the computational time of the different considered PF methods. In all cases, the HOMMP outperforms the other methods. Particularly, the N = 4 and 3 schemes are the effective and the winners are distinguished in **bold**. Only in System #4 for $\varepsilon = 10^{-6}$, NR outperforms the N = 3 scheme which is marked with underline. As it can be seen from Table 3 and Table 4, loop-based methods suffer from the solvability issue in some systems. Therefore, they will not be further evaluated in the following.

Table 4 - Comparison of the Computational Time (ms) at Base-case Scenario

Syst. No.	$\varepsilon = 10^{-6}$								$\varepsilon = 10^{-8}$							
	NR	6OM	HOMMP			Loop-based methods			NR	6OM	HOMMP			Loop-based methods		
			N = 2	N = 3	N = 4	1L	2L	3L			N = 2	N = 3	N = 4	1L	2L	3L
#1	6.8	8.3	5.8	**5.1**	6.0	14.6	107.2	130.2	8.6	10.4	7.2	7.1	**6.0**	14.5	109.5	128.1
#2	7.5	9.9	7.1	6.9	**5.9**	86.4	-	-	10.3	12.2	8.6	**7.0**	8.3	85.5	-	-
#3	8.3	9.0	7.0	6.9	**5.8**	35.3	-	-	10.9	13.9	9.8	8.7	**8.1**	35.2	-	-
#4	5.0	5.8	4.3	5.2	**3.7**	21.9	105.1	148.8	6.8	7.9	5.8	**5.2**	6.0	24.8	150.0	204.3
#5	17.8	23.3	16.8	14.8	**13.8**	-	-	557.5	23.2	31.4	21.4	21.0	**17.5**	-	-	682.6
#6	20.0	26.3	18.7	17.6	**17.3**	-	-	328.0	25.3	33.6	23.3	**9**	21.0	-	-	372.8
#7	26.2	33.0	23.0	**20.1**	20.6	150.7	-	270.2	34.2	43.5	29.8	26.1	**24.2**	165.0	-	332.6
#8	25.8	31.7	22.7	20.0	**18.6**	98.5	136.4	240.9	34.7	41.9	32.3	**28.3**	29.0	110.1	175.4	289.9
#9	45.6	54.3	43.9	43.1	**35.9**	-	-	598.0	58.6	77.4	53.3	**48.8**	51.5	-	-	661.6
#10	37.9	47.5	34.4	**30.5**	37.0	-	-	619.6	49.9	69.7	48.1	**42.4**	43.7	-	-	691.3

4.2 - Heavily loaded scenario

To examine the effect of load level on the developed PF methods, in the second scenario the specified active and reactive power of loads (i.e., P_{Lo} and Q_{Lo} in (1) and (2)) are simultaneously multiplied by a real factor namely loading level λ. The highest theoretical loading level, $\lambda_{max,t}$, represent the most demand of the system and are achieved by increasing λ in steps of 0.01 pu until "al" considered methods diverge. However, these hypothetical conditions may not be practically realized because of they violate the permissible limits of the system. Hence, in addition to $\lambda_{max,t}$, a practical

loading level limit is considered here in which the maximum and minimum operational limits, don't violate the defined values, $\pm 1\%$ of nominal frequency and $\pm 10\%$ of nominal voltage, as stated in Standard EN50160 [35]. Table 5 reports the total number of iterations at defined limit loading level. As expected, and can be deduced from this table, the convergence becomes slow as the loading level grows. The HOMMP method requires less iterations in all studied systems. Moreover, the NR and 6OM methods diverge for the Systems #5 and #10 in the case of theoretical limit loading level. For further clarification, the iteration counters at different loading level up to $\lambda_{max,p}$ is depicted in Fig. 4(a) for System #9. Trends of active and reactive power injections of resources are shown in Fig. 4(b) as well. Referring to Table 2 and this figure, this system comprises 6 DERs in which DERs #2-#4 have the same capacity, and following conclusions can be extracted: i) for the studied system, in all load level the HOMMP outperforms the NR with the schemes order of N = 4, 3 and 2, ii) Because of the conventional droop strategy, the DERs #2-#4 inject the same active power. iii) DER #1 from the base load, and subsequently DER #6 and DER #5 reach their reactive power limits from loading level λ_1 and λ_2, respectively. The iteration counters for the remain systems at different loading levels and for practical aspects, are also shown in Fig. 5. As it can be seen, the convergence becomes slow as the loading level grows. The highest convergence rate typically implies the lowest iteration counter, thus, HOMMP method with N = 4 converged in less iterations than remainder methods. Table 6 reports the computational time of the different considered PF methods at both theoretical and practical limit load levels. Like the base-case scenario, in all the studied systems, HOMMP method is generally superior to NR and 6OM methods in terms of computational speed, and this is especially evident in the N = 4 and 3 schemes. Only in Systems #6 and #7 and for theoretical aspect, NR outperforms the N = 2 scheme which are marked with underline in Table 6.

Table 5 - Limit Load Level and Total Number of Iterations at Limit Load Situation

Syt. No.	Theoretical aspect						Practical aspect					
	$\lambda_{max,t}$ (pu)	NR	6OM	HOMMP			$\lambda_{max,p}$ (pu)	NR	6OM	HOMMP		
				N = 2	N = 3	N = 4				N = 2	N = 3	N = 4
#1	2.09	96	61	50	33	25	2.09	96	61	50	33	25
#2	2.91	465	233	233	155	117	1.81	10	5	5	4	3
#3	2.90	405	202	202	135	101	1.43	10	6	5	4	3
#4	1.89	9	5	5	3	3	1.89	9	5	5	3	3
#5	6.10	*	*	*	685	514	1.73	171	86	86	57	43
#6	1.95	183	127	116	75	57	1.80	45	22	22	15	11
#7	1.67	766	401	485	285	272	1.40	47	26	26	17	13
#8	1.72	58	29	29	20	15	1.26	13	7	7	5	4
#9	1.51	234	117	117	78	59	1.21	48	24	24	16	13
#10	3.32	*	*	105	70	53	1.46	21	11	11	8	6

* Diverged.

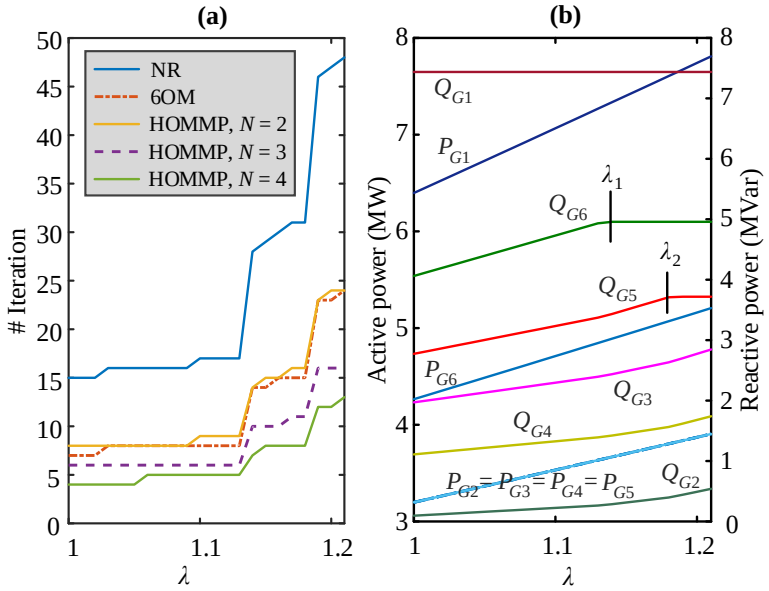

Figure 4 - (a) Total number of iterations and (b) DERs' injections for different loading levels in System #9.

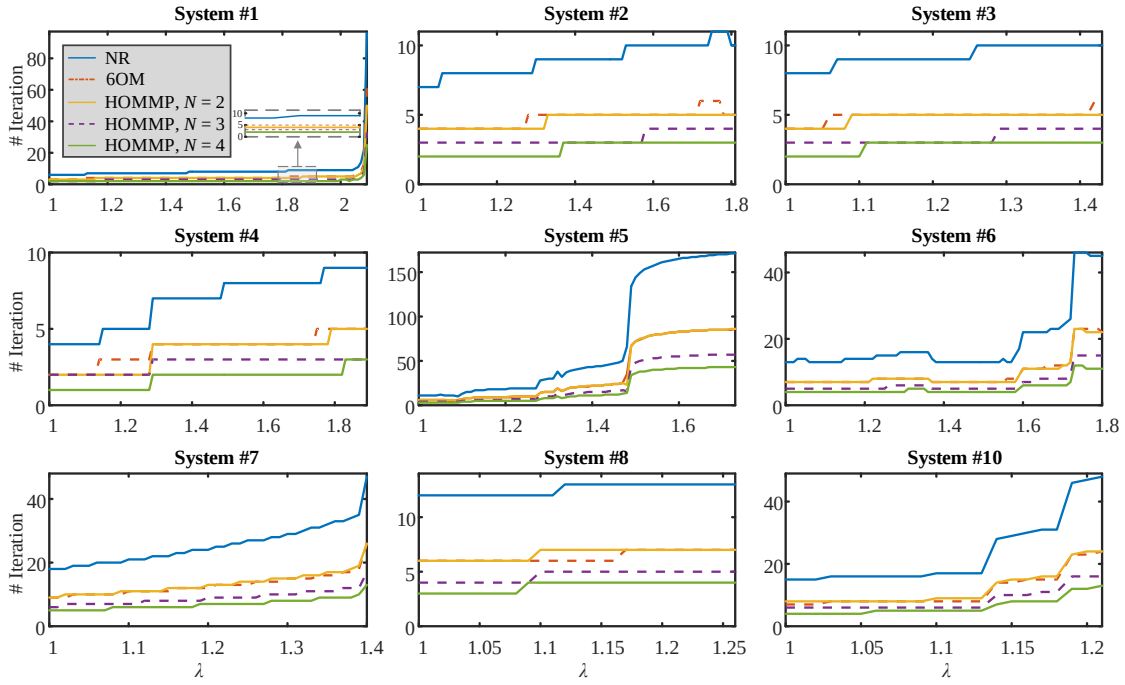

Figure 5 - Total number of iterations for different loading levels.

Table 6 - Comparison of the Computational Time (ms) at Limit Load Situation

Syt. No.	Theoretical aspect					Practical aspect				
	NR	6OM	HOMMP			NR	6OM	HOMMP		
			$N = 2$	$N = 3$	$N = 4$			$N = 2$	$N = 3$	$N = 4$
#1	96.1	133.7	80.5	69.2	**64.3**	96.1	133.7	80.5	69.2	**64.3**
#2	419.4	504.5	342.4	296.0	**274.4**	10.5	12.4	8.7	9.0	**8.4**
#3	389.1	430.4	314.8	273.0	**252.3**	10.4	14.4	8.6	9.0	**8.3**
#4	20.3	31.9	18.9	**17.0**	17.3	25.1	32.5	23.3	**20.8**	21.1
#5	-	-	-	2205.0	**2040.3**	242.7	313.4	211.0	182.4	**170.0**
#6	258.6	474.8	284.8	241.0	**223.4**	65.4	80.6	55.3	49.3	**44.8**
#7	1146.3	1422.8	1263.4	**956.9**	1125.2	64.5	92.4	62.1	53.1	**50.1**
#8	116.7	153.2	105.9	90.9	**85.7**	26.6	36.6	25.2	23.7	**23.3**
#9	1122.4	888.4	1042.1	933.2	**836.4**	143.2	179.6	130.9	**114.4**	114.9
#10	-	-	532.0	465.2	**435.7**	66.8	84.3	63.7	60.6	**56.6**

4.3 - High R/X ratio scenario

In addition to the high loading level, the robustness of the PF algorithms is usually evaluated in the condition of increased R/X ratio of the system's branches. Therefore, in the third scenario, similar to the increased loading scenario, R/X ratio of whole branches are increased by multiplying the resistances with a factor γ. Without losing any generality here only the practical situation is considered and the results for number of iterations and computational times are tabulated in tables 7 and 8, respectively. A similar trend is observed for the efficiency of the developed HOMMP method in comparison with NR and 6OM methods in this scenario. To get a better overview of computational improvement offered by the developed PF method (in the case of winner scheme) compared to the NR and 6OM methods, Figs. 6 and 7, respectively, depict this issue for three studied scenarios. It is noteworthy that the NR and 6OM methods did not converge in Systems #5 and #10 for the second scenario from the theoretical aspect.

Table 7 - Practical R/X Ratio Limit and Total Number of Iterations at this Situation

Syt. No.	$\gamma_{max,p}$ (pu)	NR	6OM	HOMMP			Syt. No.	$\gamma_{max,p}$ (pu)	NR	6OM	HOMMP		
				$N = 2$	$N = 3$	$N = 4$					$N = 2$	$N = 3$	$N = 4$
#1	8.75	14	7	7	5	3	#6	4.68	19	10	9	6	4
#2	6.01	12	6	6	4	3	#7	3.48	28	15	14	9	7
#3	4.34	11	6	6	4	3	#8	1.60	13	7	7	5	4
#4	7.79	10	6	5	2	2	#9	1.65	17	8	9	6	5
#5	4.51	90	45	46	31	23	#10	2.10	12	6	6	4	3

Table 8 - Comparison of the Computational Time (ms) at Practical R/X Ratio Limit

Syt. No.	NR	6OM	HOMMP			Syt. No.	NR	6OM	HOMMP		
			$N = 2$	$N = 3$	$N = 4$				$N = 2$	$N = 3$	$N = 4$
#1	23.4	19.7	19.2	17.8	**13.6**	#6	30.4	40.6	25.3	22.0	**18.4**
#2	17.7	16.4	14.5	12.8	**12.0**	#7	44.9	53	38.5	32.5	**31.3**
#3	18.1	16.2	16.0	14.1	**13.2**	#8	30.8	35.9	28.9	27.1	**26.9**
#4	19.4	15.7	16.0	**9.4**	11.0	#9	54.7	60.2	52.2	**46.0**	47.5
#5	129.0	181.7	114.0	100.4	**91.9**	#10	42.5	48.5	38.9	34.5	**32.4**

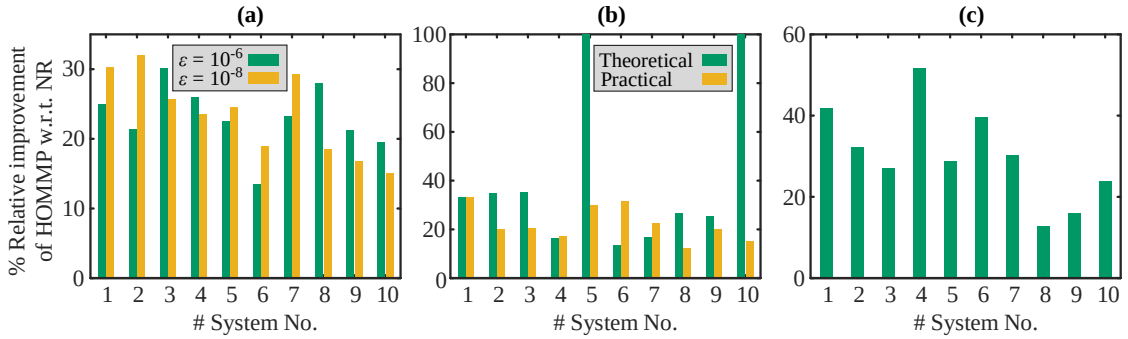

Figure 6 - Percentage computational time improvement of the developed HOMMP method in best scheme w.r.t NR method at: (a) Base-case scenario, (b) Limit loading level, and (c) Practical limit of increased R/X ratio scenario.

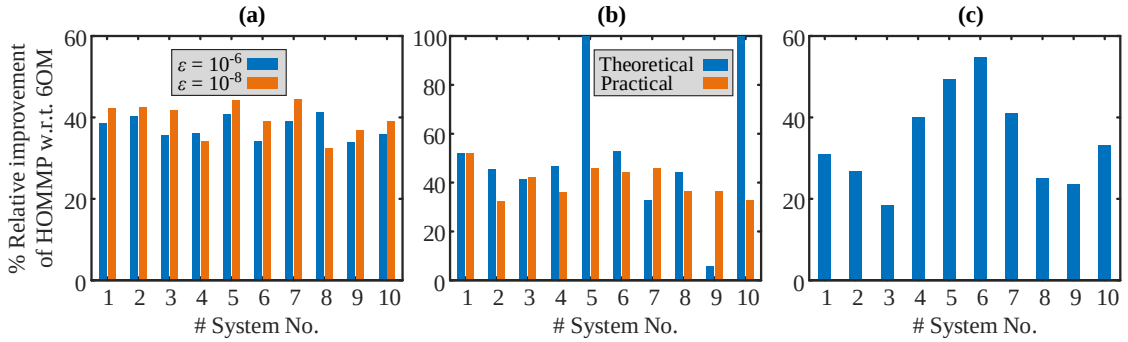

Figure 7 - Percentage computational time improvement of the developed HOMMP method in best scheme w.r.t 6OM method at: (a) Base-case scenario, (b) Limit loading level, and (c) Practical limit of increased R/X ratio scenario.

5 - Conclusions and future works

A novel Newton-like solver for Power-Flow solution in isolated Microgrids has been presented. The new proposal is based on the Modified Midpoint method and presents a multi-step structure by which is able to reach $N+1$ order of convergence (where N is the number of steps involved) whereas the computational burden is preserved light and comparable to the Newton-Raphson technique.

Superior features of the new method in comparison with the Newton-Raphson solver have been firstly demonstrated by using a theoretical efficiency index and posteriorly by extensive simulations. In this last regard, various numerical results have been presented on different small-, and large-scale benchmark microgrids. In all cases, the new method was more efficient than the Newton-Raphson solver, which is considered the most conventional Power-Flow solver. For more verification, the proposed method is also compared with the recently developed loop-base methods and a method with convergence rate of order 6. Results have also shown that the developed methodology is able to calculate reliable results under different demanding scenarios like heavy loading levels or high R/X ratio conditions.

Future works will be focused on studying the applicability of the developed solution scheme in other power system tools, and adaptation of this method for unbalanced three-phase networks.

References

[1] F. Milano, *Power System Modelling and Scripting*. New York, NY, USA: Springer, 2010.

[2] P. R. Bijwe and S. M. Kelapure, "Nondivergent fast power flow methods," *IEEE Trans. Power Syst.*, vol. 18, no. 2, pp. 633-638, May 2003, doi: 10.1109/TPWRS.2003.810905.

[3] M. Tostado-Véliz, S. Kamel, T. Alquthami and F. Jurado, "A Three-Stage Algorithm Based on a Semi-Implicit Approach for Solving the Power-Flow in Realistic Large-Scale ill-Conditioned Systems," *IEEE Access*, vol. 8, pp. 35299-35307, 2020, doi: 10.1109/ACCESS.2020.2975058.

[4] W. H. Kersting, *Distribution System Modeling and Analysis*, 2nd ed. Boca Raton, FL, USA: CRC Press, 2006.

[5] M. Tostado-Véliz, S. Kamel and F. Jurado, "Promising Framework Based on Multistep Continuous Newton Scheme for Developing Robust PF Methods", *IET Gener. Transmiss. Distrib.*, vol. 14, no. 2, pp. 265-274. doi: 10.1049/iet-gtd.2019.1077.

[6] M. Tostado-Véliz, P. Arévalo and F. Jurado, "A comprehensive electrical-gas-hydrogen Microgrid model for energy management applications," *Energy Convers. Manag.*, vol. 228, Jan. 2021, Art. no. 113726, doi: 10.1016/j.enconman.2020.113726.

[7] M. Bayat, K. Sheshyekani, and A. Rezazadeh, "A unified framework for participation of responsive end-user devices in voltage and frequency control of the smart grid," *IEEE Trans. Power Syst.*, vol. 30, no. 3, pp. 1369-1379, May 2015, doi: 10.1109/TPWRS.2014.2344133.

[8] F. Mumtaz *et al.*, "A Novel Approach to Solve Power Flow for Islanded Microgrids Using Modified Newton RaphsonWith Droop Control of DG," *IEEE Trans. Sustain. Energy*, vol. 7, no. 2, pp. 493-503, Apr. 2016, doi: 10.1109/TSTE.2015.2502482.

[9] M. Bayat *et al.*, "Coordination of Distributed Energy Resources and Demand Response for Voltage and Frequency Support of MV Microgrids," *IEEE Trans. Power Syst.*, vol. 31, no. 2, pp. 1506-1516, Mar. 2016, doi: 10.1109/TPWRS.2015.2434938.

[10] F. Hameed, M. Al Hosani and H. H. Zeineldin, "A Modified Backward/Forward Sweep Load Flow Method for Islanded Radial Microgrids," *IEEE Trans. Smart Grid*, vol. 10, no. 1, pp. 910-918, Jan. 2019, doi: 10.1109/TSG.2017.2754551.

[11] M. M. A. Abdelaziz *et al.*, "A Novel and Generalized Three-Phase Power Flow Algorithm for Islanded Microgrids Using a Newton Trust Region Method," *IEEE Trans. Power Syst.*, vol. 28, no. 1, pp. 190-201, Feb. 2013, doi: 10.1109/TPWRS.2012.2195785.

[12] M. H. Moradi, V. H. Foroutan and M. Abedini, “Power flow analysis in islanded Micro-Grids via modeling different operational modes of DGs: A review and a new approach,” *Renew. Sustain. Energy Rev.*, vol. 69, pp. 248-262, Mar. 2017, doi: 10.1016/j.rser.2016.11.156.

[13] G. C. Kryonidis *et al.*, “Power Flow of Islanded AC Microgrids: Revisited,” *IEEE Trans. Smart Grid*, vol. 9, no. 4, pp. 3903-3905, Jul. 2018, doi: 10.1109/TSG.2018.2799480.

[14] E. O. Kontis et al., “Power Flow Analysis of Islanded AC Microgrids,” *2019 IEEE Milan PowerTech*, Milan, Italy, 2019, pp. 1-6, doi: 10.1109/PTC.2019.8810612.

[15] A. Kumar *et al.*, “Current injection-based Newton Raphson power-flow algorithm for droop-based islanded microgrids,” *IET Gener. Transmiss. Distrib.*, vol. 13, no. 23, pp. 5271-5283, Dec. 2019, doi: 10.1049/iet-gtd.2019.0575.

[16] M. A. Allam, A. A. Hamad and M. Kazerani, “A Generic Modeling and Power-Flow Analysis Approach for Isochronous and Droop-Controlled Microgrids,” *IEEE Trans. Power Syst.*, vol. 33, no. 5, pp. 5657-5670, Sept. 2018, doi: 10.1109/TPWRS.2018.2820059.

[17] A. Kumar et al., “A Nested-Iterative Newton-Raphson based Power Flow Formulation for Droop-based Islanded Microgrids,” *Elect. Power Syst. Res.*, vol. 180, Mar. 2020, Art. no. 106131, doi: 10.1016/j.epsr.2019.106131.

[18] G. Diaz and C. Gonzalez-Moran, “Fischer-Burmeister-Based Method for Calculating Equilibrium Points of Droop-Regulated Microgrids,” *IEEE Trans. Power Syst.*, vol. 27, no. 2, pp. 959-967, May 2012, doi: 10.1109/TPWRS.2011.2175754.

[19] P. Henneaux and D. S. Kirschen, “Probabilistic security analysis of optimal transmission switching,” *IEEE Trans. Power Syst.*, vol. 31, no. 1, pp. 508-517, Jan. 2016, doi: 10.1109/TPWRS.2015.2409152.

[20] M. Bayat, K. Ghaseminezhad and A. A. Ghadimi, “An efficient iterative approach for power flow solution of droop-controlled islanded AC microgrids through conventional methods,” *Int. J. Elect. Power Energy Syst.*, vol. 130, Sept. 2021, Art. no. 106962, doi: 10.1016/j.ijepes.2021.106962.

[21] C. Chun and B. Neta, “Developing high order methods for the solution of systems of nonlinear equations,” *Appl. Math. Comput.*, vol. 342, pp. 178-190, Feb. 2019, doi: 10.1016/j.amc.2018.09.032.

[22] M. Okamura et al., “A new power flow model and solution method - Including load and generator characteristics and effects of system control devices,” *IEEE Trans. Power Appar. Syst.*, vol. PAS-94, no. 3, pp. 1042–1050, May/Jun. 1975, doi: 10.1109/T-PAS.1975.31938.

[23] J. M. Guerrero et al., “Hierarchical control of droop-controlled AC and DC microgrids-A general approach toward standardization,” *IEEE Trans. Ind. Electron.*, vol. 58, no. 1, pp. 158–172, Jan. 2011, doi: 10.1109/TIE.2010.2066534.

[24] W.B. Gragg, "Repeated extrapolation to the limit in the numerical solution of ordinary differential equations," *SIAM J. Numer. Anal.*, vol. 2, pp. 384-403, 1965.

[25] F. Milano, "Continuous Newton's Method for Power Flow Analysis," *IEEE Trans. Power Syst.*, vol. 24, no. 1, pp. 50-57, Feb. 2009, doi: 10.1109/TPWRS.2008.2004820.

[26] T. Alharbi, M. Tostado-Véliz, O. Alrumayh and F. Jurado, "On Various High-Order Newton-Like Power Flow Methods for Well and Ill-Conditioned Cases," *Mathematics*, vol. 9, no. 17, p. 2019, Aug. 2021, doi: 10.3390/math9172019.

[27] A. Cordero, J.L. Hueso, E. Martínez and J.R. Torregrosa, "A modified Newton-Jarratt's composition," *Numer. Algor.*, vol. 5, no. 1, pp. 87-99, Sept. 2010, doi: 10.1007/s11075-009-9359-z.

[28] R. A. Jabr, "High-Order Approximate Power Flow Solutions and Circular Arithmetic Applications," *IEEE Trans. Power Syst.*, vol. 34, no. 6, pp. 5053-5062, Nov. 2019, doi: 10.1109/TPWRS.2019.2922269.

[29] J. E. Tate and T. J. Overbye, "A comparison of the optimal multiplier in polar and rectangular coordinates," *IEEE Trans. Power Syst.*, vol. 20, no. 4, pp. 1667-1674, Nov. 2005, doi: 10.1109/TPWRS.2005.857388.

[30] M. Tostado-Véliz, S. Kamel, F. Jurado and F. J. Ruiz-Rodríguez, "On the Applicability of Two Families of Cubic Techniques for Power Flow Analysis," *Energies*, vol. 14, no. 14, p. 2021, July 2021, doi: 10.3390/en14144108

[31] R. D. Zimmerman, C. E. Murillo-Sánchez, and R. J. Thomas, "Matpower: Steady-State Operations, Planning and Analysis Tools for Power Systems Research and Education," *IEEE Trans. Power Syst.*, vol. 26, no. 1, pp. 12-19, Feb. 2011, doi: 10.1109/TPWRS.2010.2051168.

[32] *Benchmark Systems for Network Integration of Renewable and Distributed Energy Resources*, 575, CIGRE, 2014. [Online]. Available: http://www.e-cigre.org/publication/575-benchmark-systems-for-network-integration-of-renewable-and-distributed-energy-resources, (Accessed Aug. 31, 2021).

[33] A. A. A. El-Ela, R. A. El-Sehiemy and A. S. Abbas, "Optimal Placement and Sizing of Distributed Generation and Capacitor Banks in Distribution Systems Using Water Cycle Algorithm," *IEEE Syst. J.*, vol. 12, no. 4, pp. 3629-3636, Dec. 2018, doi: 10.1109/JSYST.2018.2796847.

[34] D. Zhang, Zh. Fu, L. Zhang, "An improved TS Algorithm for Loss-minimum Reconfiguration in Large-scale Distribution Systems," Elect. Power Syst. Res., vol. 77, 2007, pp. 685–694, doi: 10.1016/j.epsr.2006.06.005.

[35] *Voltage Characteristics of Electricity Supplied by Public Distribution Networks*, EN Standard 50160, 2010.